Spectroscopy and high-spin structure of ^{210}Fr: Isomerism and potential evidence for configuration mixing

V. Margerin,[*] G. J. Lane, G. D. Dracoulis,[†] N. Palalani,[‡] M. L. Smith, and A. E. Stuchbery

Department of Nuclear Physics, Research School of Physical Sciences and Engineering, The Australian National University, Canberra, Australian Capital Territory 0200, Australia

(Received 8 February 2016; published 8 June 2016)

The structure of ^{210}Fr has been established up to an excitation energy of $\sim$5.5 MeV and spins of $\sim$25$\hbar$, via time-correlated γ-ray spectroscopy and using the ^{197}Au(^{18}O,$5n$)^{210}Fr reaction with pulsed beams at an energy of 97 MeV. A significantly different level scheme has been obtained compared to previous publications. Several isomers are reported here, including a $J^{\pi} = (23)^+$, $\tau = 686(9)$-ns state at 4417 keV and a 10^-, 29.8(11)-ns state at 1113 keV. The former isomer has been associated with the $\pi(h_{9/2}^3 i_{13/2}^2)\nu(p_{1/2}^{-2} f_{5/2}^{-1})$ configuration and decays via proposed $E3$ transitions with strengths of 8.4(3) and 21.2(8) W.u. There are only very few known cases of a high-spin isomer decaying via two parallel $E3$ transitions. Indeed, this is not seen in other Fr nuclei, and consequently these strengths differ from related decays in the neighboring isotopes. However, by examining the systematics of $E3$ transitions in trans-lead nuclei, we suggest that the weaker of the two transitions decays to a mixed 20^- state. Systematics of the 10^- isomer are also discussed. Comparisons are made between the observed spectrum of states and those predicted from semiempirical shell-model calculations.

I. INTRODUCTION

Nuclei near the $Z = 82$, $N = 126$ shell closures provide an important testing ground for the shell model of nuclei that describes nuclear properties in the framework of single- and multiparticle excitations in a spherical field. However, it is well known [1] that coupling to the collective motion arising from the 3^- octupole vibration at 2615 keV in ^{208}Pb also plays a crucial role in this region. This coupling is strongest between specific multiparticle proton or neutron excitations, resulting in the frequent occurrence of $E3$ transitions, a phenomenon that can be used as a signature of particular configuration changes. Although strongly enhanced compared to single-particle transition strengths, the high multipolarity usually results in isomerism.

Full-scale shell-model calculations become less tractable for high-spin states, because the many available spin orbits in the basis space cause impractically large dimensions for calculation. Semiempirical shell-model approaches that rely on the availability of experimental two-body residual interactions, or theoretical values in their absence, have been widely and successfully used around ^{208}Pb. Extensive compilations of interactions are available, including the theoretical values of Kuo and Herling [2] and various experimental values obtained from the study of multiplets in nuclei around ^{208}Pb that are augmented occasionally as more information becomes available (see, for example, Refs. [3–6], and references therein). Calculations can yield an accuracy of better than tens of keV (see, for example, Ref. [7]), particularly for favored configurations that can often result in yrast isomers.

A number of francium isotopes with $N \leqslant 126$ have been successfully described within this shell-model framework, including ^{211}Fr, ^{212}Fr, and ^{213}Fr, as reported by Byrne *et al.* [8], with ^{213}Fr extended later to $J = 65/2\hbar$ [9]. The isotopes just above the closed shell are also well understood up to high spins, $J \sim 36\hbar$ in ^{214}Fr [10] and $J \sim 41/2\hbar$ in ^{215}Fr [11]. Pear-shaped octupole deformation develops with an increasing number of neutrons [12], as reported for francium isotopes with $A \geqslant 216$ (see, for example, Ref. [13]).

The situation for the more neutron-deficient cases with $A < 211$ is less clear, partly because fission competition increases rapidly, resulting in both lower yields and lower spin input, and partly because the additional neutron holes result in more fragmented level schemes. The original assignments for ^{209}Fr and ^{210}Fr [14] were subsequently shown to be erroneous by Dracoulis *et al.*, who reported a definitive high-spin scheme for ^{209}Fr [15] and also levels up to $J \sim 16$ $\hbar$ in ^{208}Fr [16]. The lighter isotopes, such as ^{207}Fr and, especially, ^{206}Fr are expected to develop deformation at high spins [17], although there is no definite study to support this. Until recently, little was known of the intervening isotope ^{210}Fr. Unfortunately, it turns out that the new results reported here are in substantial disagreement with the work on ^{210}Fr carried out in parallel to the present study and recently published by Kanjilal *et al.* [18]. Preliminary results of our study were reported earlier [19].

II. EXPERIMENTAL PROCEDURES AND ANALYSIS

The ^{197}Au(^{18}O,$5n$)^{210}Fr reaction, at a beam energy of 97 MeV, was used with a 5.5 mg/cm^2 gold target, sufficiently thick to stop most of the recoils. A beam with pulses 1 ns wide separated by 1712 ns was delivered by the 14UD Pelletron accelerator at the Australian National University for

―――――――
[*]Present address: School of Physics and Astronomy, The University of Edinburgh, Edinburgh EH9 3JZ, UK; vincent.margerin@ed.ac.uk
[†]Deceased.
[‡]Present address: Department of Physics, Faculty of Science, University of Botswana, Gaborone, Botswana.

the main γ-γ time measurements. For a subsequent study of the long-lived, high-spin isomeric state, a macroscopically chopped beam with on/off periods of 1 and 9 μs was used, in conjunction with an in-beam veto to isolate out-of-beam decays.

Time-correlated γ-ray spectroscopy was performed with the CAESAR array [20], consisting of six Compton-suppressed high-purity germanium (HPGe) detectors positioned in pairs in the vertical plane at angles of $\pm 34.75°$, $\pm 48.75°$, and $\pm 82.75°$, with respect to the beam direction, allowing the measurement of angular anisotropies. Another three Compton-suppressed HPGe detectors and two (unsuppressed) low-energy photon spectrometers (LEPS) are placed close to the horizontal plane.

A variety of techniques were used to measure lifetimes, ranging from the microsecond region, down to a few nanoseconds. Complementary, and in some cases, independent, results were obtained through either direct timing of γ rays with respect to the pulsed or chopped beams or via measurement of the time difference between γ rays. In the latter case, intermediate-time spectra were obtained from γ-γ time cubes with gates on transitions above and below the state of interest, to isolate individual state lifetimes. Details and applications of the techniques developed for the present experimental system can be found in a number of publications, for example, Refs. [3,21,22].

For the angular anisotropies, singles γ-ray results were used where possible, or otherwise, to avoid contamination, γ-γ coincidence data were used. In the latter case, coincidence matrices were constructed with one axis composed of γ rays observed in any of the three pairs of detectors at particular angles in the vertical plane, while the other axis contained coincident γ rays from any of the nine HPGe detectors. With only three angles available, the A_4 coefficient was set to zero when fitting the anisotropies to an expansion in Legendre polynomials. Hence, these values can only be used as a guide to multipolarity assignments and there is insufficient information to extract accurate mixing ratios.

III. RESULTS

A. Isotopic assignments

Isotopic assignments were based on excitation function yields and coincidences between candidate lines and characteristic francium x rays. Under the present conditions, a relatively low yield of γ rays from ^{209}Fr ($6n$ channel) was observed, whereas all the transitions in ^{211}Fr reported by Byrne *et al.* [8] ($4n$ channel) were seen. In principle, with the energy optimized for the $5n$-evaporation channel (allowing for the energy loss in the target), ^{210}Fr lines should be clear. However, the situation is complicated by a number of factors. As was pointed out by Dracoulis *et al.* [15], several of the main low-lying transitions in ^{210}Fr overlap with lines in ^{210}Rn , ^{206}At, and ^{206}Po, all of which are decay products of ^{210}Fr, and several of which can also be populated directly via proton and α-particle evaporation channels. Another factor that reduces the relative intensity of individual lines is the relatively high fragmentation

of the level scheme of ^{210}Fr at low spin, compared to the other products.

B. ^{210}Fr level scheme

The level scheme of ^{210}Fr established from the present study is shown in Fig. 1, and the list of γ rays observed is presented in Table I together with in-beam relative intensities, angular anisotropies, and level scheme placements. Several low-spin states and associated transitions have been assigned to ^{210}Fr from a study of the α decay of ^{214}Ac [23]. One of these states at 754 keV is likely to be associated with the 754-keV state that we observe. The differences between Fig. 1 and the level scheme given in Ref. [18] are too numerous to discuss in detail. The following section only provides evidence to justify the present level scheme, whereas a more complete comparison that directly addresses Ref. [18] can be found in Ref. [24].

1. Transitions below the state at 2206 keV

Key features of the decay scheme can be observed from the prompt, in-beam (-25 to $+150$ ns), coincidence spectra shown in Fig. 2. The 816.8-keV γ ray is in coincidence with all the transitions that feed the 1626.6-keV state (top panel), but there are at least four other strong parallel decay paths from the 1626.6-keV state to ground. The γ-rays in all those paths, including the 816.8/721.2-keV, 519.6(544.4)/793.0/289.1-keV, 519.6(544.4)/902.5/143.2-keV, and 753.8(729.0)/693.2/143.2-keV cascades, are evident in the coincidence spectrum obtained with a gate on the 257-keV line, as shown in the bottom panel of Fig. 2, while their placements in separate cascades are proven by coincidence gates on the individual paths, available in Ref. [24]. The 1626.6-keV state is predominantly fed through the 256.9/203.5/118.9-keV γ-ray cascade from the decay of the 2205.9-keV state.

Several low-energy unobserved transitions are placed in the scheme below the 1626.6-keV state that is fed by the 118.9-keV transition. The coincidence relationships between the 118.9-keV transition and the multiple decay paths to the ground state, together with the presence of a range of crossover transitions and a considerable body of cross-coincidence relationships between the parallel decay pathways, allows unambiguous placement of the unobserved transitions, including a 24.8-keV transition that connects the 24.8-keV state to the ground state, a 36.5-keV transition from the 1626.6-keV state to the 1590.1-keV state, and an 87.8-keV transition between the 841.6- and 753.8-keV states. Again, complete details can be found in Ref. [24].

2. Transitions above the state at 2206 keV

The presence of the 573.5- and 663.3-keV lines in most of the out-of-beam coincidence spectra and their absence in the in-beam spectra was strongly suggestive of a long-lived isomer lying at high spin. The existence of this isomer enabled a separation of in-beam and out-of-beam transitions, leading to high sensitivity, and allowed uncontaminated gates to be placed on many transitions, greatly easing the construction of both the high-spin and low-spin scheme.

FIG. 1. Level scheme for ^{210}Fr from the present study. The transition width indicates the prompt γ-ray intensity. States with a long lifetime are drawn with thicker lines while numbers below the energy labels indicate the state lifetimes. Transition energies in brackets and with no γ-ray intensity given are inferred from coincidence relationships and are not observed directly.

TABLE I. Properties of transitions assigned to ^{210}Fr.

E_γ [a]	I_γ	A_2/A_0	E_i	E_f	J_i^π	J_f^π	E_γ [a]	I_γ	A_2/A_0	E_i	E_f	J_i^π	J_f^π
11.5			3129.1	3117.6	16$^-$		405.6	71(7)	$-0.54(6)$				
17.2			2017.9	2000.7	12$^-$	11$^-$	479.4	10(4)		3103.4	2623.8	16$^{(-)}$	14$^-$
24.8			24.8	0	7$^+$	6$^+$	486.4	86(6)	$-0.34(4)$	3843.7	3357.3	20$^-$	19$^-$
25.9			3129.1	3103.2	16$^-$	15$^-$	495.5			3822.0	3326.5		19$^-$
30.8			3357.3	3326.5	19$^-$	18$^-$	495.7	62(3)		1337.4	841.6	10$^+$	9$^+$
36.5			1626.6	1590.1	12$^+$	11$^+$	505.2	90(8)	$-0.69(4)$	3040.7	2535.5	17$^-$	16$^-$
63.8	62(8)		1626.6	1562.8	12$^+$	11$^+$	517.2	5(2)		3843.7	3326.5	20$^-$	18$^-$
87.8			841.6	753.8	9$^+$	8$^+$	519.6	547(15)	$-0.44(3)$	544.4	24.8	8$^+$	7$^+$
95.1			1949.1	1854.0	14$^+$	(13)$^+$	528.6	185(7)[e]		1641.2	1112.6	11$^{(-)}$	10$^-$
113.9			3103.2	2989.3	15$^-$	14$^-$	528.6	92(4)[e]		2169.8	1641.2		11$^-$
118.9	125(7)	$+0.36(4)$[b]	1745.5	1626.6	14$^+$	12$^+$	544.4	172(7)	$+0.40(3)$[c]	544.4	0	8$^+$	6$^+$
143.2	52(4)	$-0.32(4)$[c]	1590.1	1446.9			559.1	28(3)	$-0.73(3)$[d]	1671.7	1112.6	11$^-$	10$^-$
154.8	15(5)						564.5	3(2)		4981.7	4417.2		23$^+$
163.3	50(5)	$-0.29(4)$	3129.2	2966.0	19$^{(-)}$	18$^{(-)}$	573.5	13(5)	$+0.35(7)$	4417.2	3843.7	23$^+$	20$^-$
173.7	36(5)	$-0.36(4)$[c]					586.4	5(3)		5003.6	4417.2		23$^+$
203.5	355(9)	$-0.39(4)$[d]	1949.1	1745.5	15$^+$	14$^+$	589.5	36(5)	$-0.69(9)$[c]	3125.0	2535.5	18$^{(-)}$	17$^-$
225.4	90(8)	$-0.21(4)$	1562.8	1337.4	11$^+$	10$^+$	663.6	18(6)	$+0.41(6)$	4417.2	3753.9	23$^+$	20$^-$
227.3	78(8)	$+0.37(4)$	1853.9	1626.6	13$^{(+)}$	12$^+$	678.4						
250.7	32(5)	$-0.26(7)$	4094.4	3843.7	21$^-$	20$^-$	693.2	115(4)	$+0.16(4)$[c]	1446.9	753.8	10$^+$	8$^+$
256.9	1000(25)	$-0.27(3)$[d]	2205.9	1949.0	16$^-$	15$^+$	716.5	55(10)		2343.1	1626.6		
265.6	51(5)	$-0.30(7)$[c]					717.8	48(8)	$+0.33(10)$[c]				
271.0	346(9)	$-0.13(4)$[d]	1112.6	841.6	10$^-$	9$^+$	721.2	803(20)	$+0.27(3)$[d]	1562.8	841.6	11$^+$	9$^+$
280.4	119(3)	$-0.11(4)$[d]	2298.3	2017.9	13$^-$	12$^-$	729.0	39(4)		753.8	24.8	8$^+$	7$^+$
285.8	71(5)	$-0.35(2)$[c]	3326.6	3040.8	18$^-$	17$^-$	753.8	166(8)	$+0.37(3)$[c]	753.8	0	8$^+$	6$^+$
289.1	268(9)	$+0.29(3)$	1626.6	1337.4	12$^+$	10$^+$	774.5	31(6)	$+0.42(21)$[f]	3117.6	2343.1		
291.6	71(8)	$-0.19(3)$	3811.6	3520.0	18$^{(-)}$	17$^{(-)}$	784.4	27(5)	$+0.49(13)$[g]	2954.2	2169.8		
304.2	64(6)	$-0.32(4)$	2049.7	1745.5	15$^{(+)}$	14$^+$	791.0	85(7)	$+0.25(10)$[f]	3326.5	2535.5	18$^-$	16$^-$
316.6	156(7)	$+0.34(3)$	3357.3	3040.7	20$^-$	18$^-$	793.0	495(12)	$+0.33(4)$	1337.4	544.4	10$^+$	8$^+$
324.5	6(3)		4741.7	4417.2		23$^+$	796.5						
325.5	84(3)	$-0.29(4)$	2623.8	2298.3	14$^-$	13$^-$	816.8	1259(28)	$+0.28(2)$	841.6	24.8	9$^+$	7$^+$
329.6	182(7)	$-0.42(4)$	2535.5	2205.9	16$^-$	15$^-$	834.8	315(10)	$+0.36(3)$[c]	3040.7	2205.9	17$^-$	15$^-$
337.8	23(4)		4432.2	4094.4	22$^{(-)}$	21$^-$	867.9	51(4)	$-0.35(4)$[d]	1709.1	841.6		10$^+$
340.2	58(7)	$-0.28(5)$	4094.4	3753.9	21$^-$	20$^-$	885.7	37(2)	$(-0.16(16)$[d]$)$	1727.3	841.6		10$^+$
346.2	12(5)		2017.9	1671.7	12$^-$	11$^{(-)}$	888.1	51(3)	$+0.77(27)$[g]	2000.7	1112.6	11$^-$	10$^-$
365.5	84(3)	$-0.54(3)$[d]	2954.3	2623.8	15$^-$	14$^-$	902.5	200(6)	$+0.32(3)$	1446.9	544.4	10$^+$	8$^+$
376.7	8(4)		2017.9	1641.2	12$^-$	11$^{(-)}$	923.2	61(6)	$-0.33(3)$	3129.1	2205.9	16$^{(-)}$	15$^-$
385.8	59(5)	$-0.37(3)$	2591.7	2205.9	16$^{(-)}$	15$^-$	1096.9	8(3)		5514.1	4417.2	(26$^-$)	23$^+$
390.8	134(8)	$-0.41(4)$	3520.0	3129.2	17$^{(-)}$	16$^-$	1176.3	92(4)	$+0.27(5)$	2017.9	841.6	12$^-$	9$^+$
396.6	112(8)	$-0.28(3)$	3753.9	3357.3	20$^-$	19$^-$							

[a]Transition energies in italics are unobserved transitions inferred from coincidence information.
[b]Angular anisotropy in a 519.6-keV gated spectrum.
[c]Angular anisotropy in a 256.9-keV gated spectrum.
[d]Angular anisotropy in a 816.8-keV gated spectrum.
[e]The intensity was obtained for the doublet of transitions at 528.6 keV and (arbitrarily) apportioned with 2/3 for the lower transition and 1/3 for the higher transition.
[f]Angular anisotropy in the sum of gates on intense, low-lying $E2$ transitions. Specific transitions are chosen depending upon the contamination in the gate.
[g]Angular anisotropy in a 271.0-keV gated spectrum.

The out-of-beam spectrum with a gate on the 257-keV line, shown in Fig. 3 (cf. Fig. 2), reveals two paths above the short-lived isomer at 2205.9 keV, proceeding through the 834.8/316.7- and 329.6.7/791.0(505.2/285.8)-keV γ-ray cascades. These cascades are also evident in the out-of-beam coincidence spectra for the 574- and 663-keV lines, presented in Fig. 4. At first glance, all the transitions in these two spectra have the same relative intensities; however, a closer look reveals subtle differences in, for example, the ratio of the intensities of the 505/520- and 317/300-keV pairs of transitions and a slight shift in the energy of the 791.0/793.0-keV doublet towards 791.0 keV in the spectrum for the 574-keV
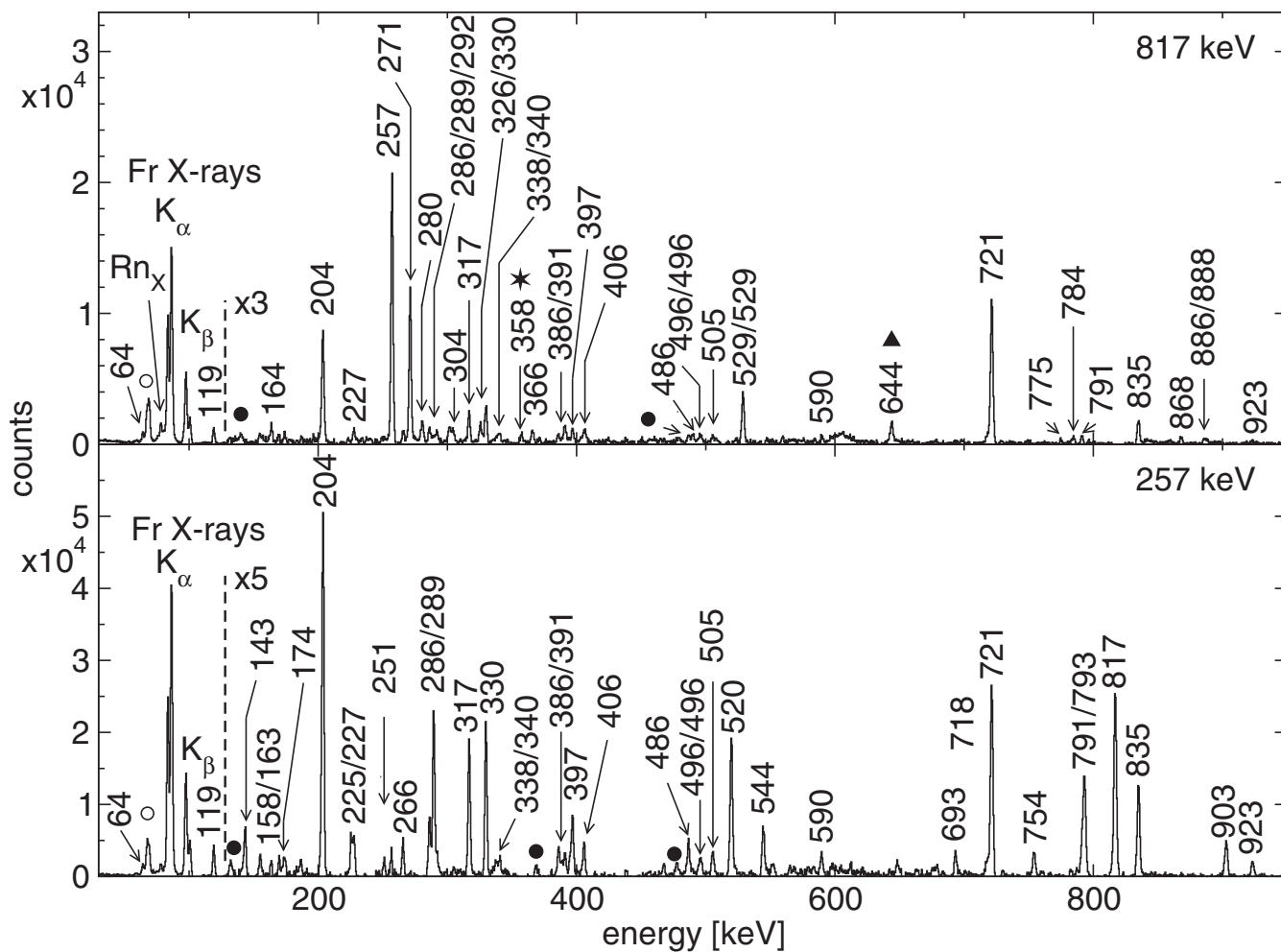
FIG. 2. Time-correlated γ-ray coincidence spectra, measured in beam (-25 ns to $+150$ ns), with energy gates as indicated. Note that in both spectra the γ rays at 574 and 663 keV, from the decay of the 686(9)-ns isomer, are not observed. The triangle and star indicate ^{210}Rn and ^{211}Fr contaminants, respectively. The solid circles label subtraction artifacts or unidentified contaminants, while the open circle corresponds to the target x rays that appear owing to random coincidences.
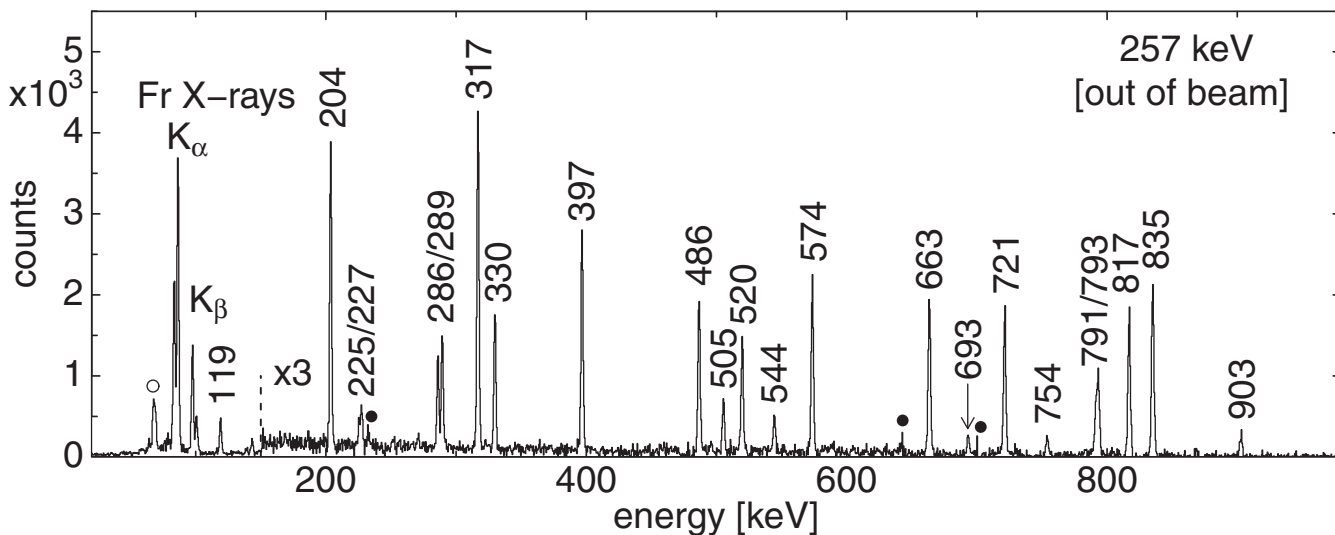

FIG. 3. Out-of-beam γ-ray coincidence spectrum for the 257-keV transition. Solid and open circles mean the same as in Fig. 2.
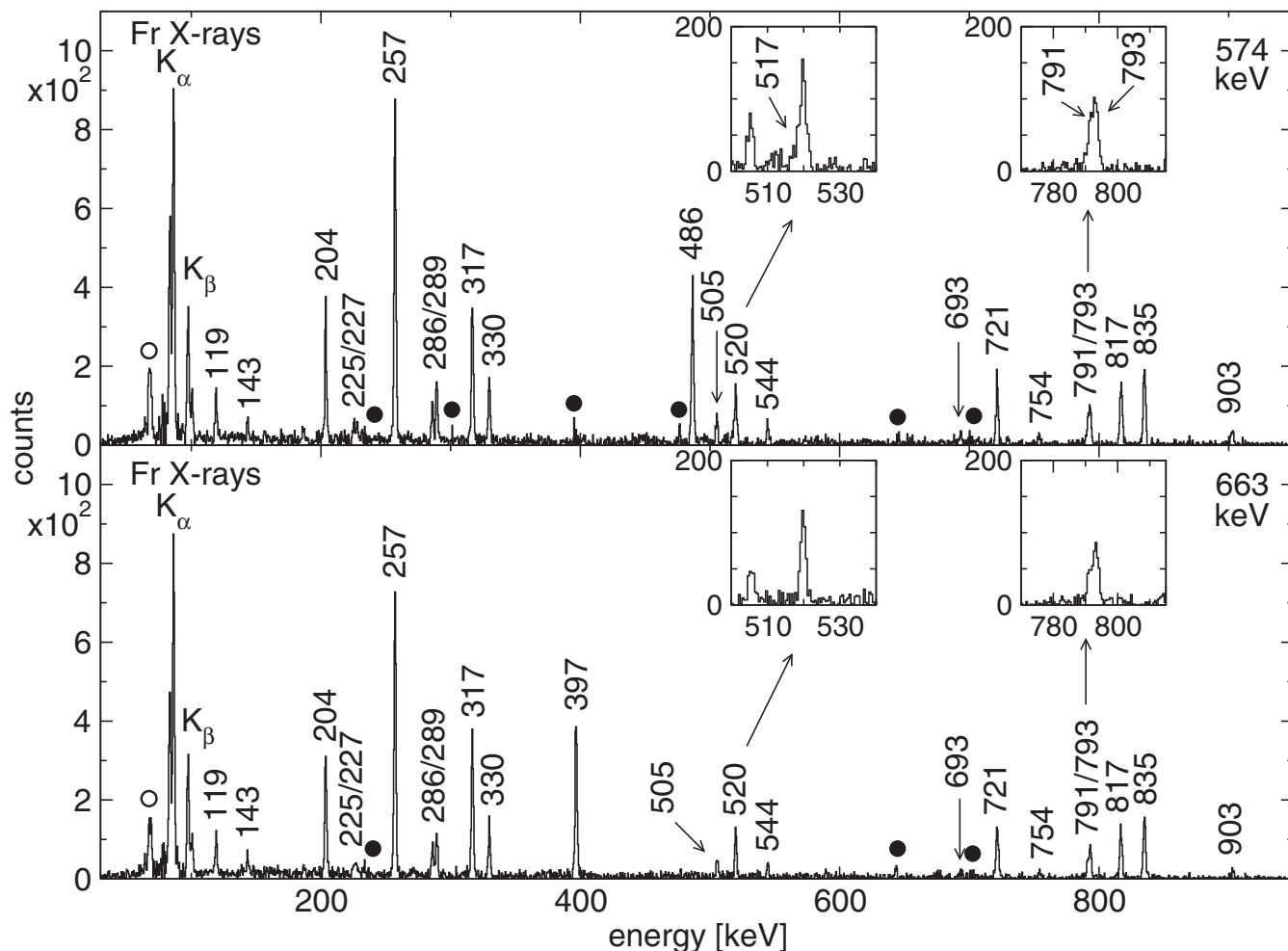
FIG. 4. Out-of-beam γ-ray coincidence spectra for the 574-keV (top panel) and 663-keV (bottom panel) transitions. Solid and open circles have the same meanings as in Fig. 2.

gate. These observations lead to the placement of a weak 517.2-keV transition (see inset in the top panel of Fig. 4) connecting the 3843.7- and 3326.5-keV states.

A weak (340.2, 250.7)/337.8-keV γ-ray cascade seen in Fig. 2 bypasses the isomer at 4417.2 keV. Another important transition is the 923.2 keV γ-ray evident in the prompt coincidence spectra shown in Fig. 2. This line is placed as a decay from the 3129.1-keV state to the 2206.9-keV state, one of the few connections between the right-hand side of the level scheme in Fig. 1 to the more strongly populated states on the left.

3. Transitions above the state at 4417 keV

Four lines at 324.5, 564.5, 586.4, and 1096.9 keV are assigned as feeding the 686-ns isomer at 4417 keV on the basis of early-delayed coincidences with strong transitions in its decay; see Fig. 5. They do not appear to be in coincidence with each other and hence are proposed as parallel feeds into the isomer.

4. States associated with the 1113-keV, 10⁻ isomer

As depicted in Fig. 1, the level scheme largely separates into states fed by the 4417-keV isomer (discussed above) and

those that branch into, or only decay to, the 1113-keV state drawn on the right-hand side. These can be isolated initially by gating on the delayed 271-keV transition that depopulates the 1113-keV, 30-ns isomer. Although not presented here, the spectrum produced in this way has prominent lines at 528.6, 888.1, 280.4, 365.5, 325.5, 291.6, and 390.8 keV and does not show the 1176.3-keV line, which is placed as a parallel branch from the 2018-keV, 8-ns isomer to the 842-keV state. The ordering of the 280.4-, 325.5-, and 365.5-keV transitions above the 2018-keV state is based largely on coincidence intensities, while the 3103- and 3129-keV states are fixed through several branches. The 528.6-keV line is observed to be in self-coincidence leading to the proposed cascade of two transitions of the same energy.

C. Conversion coefficients

A number of conversion coefficients were extracted from intensity balances. Most of these measurements were made by summing out-of-beam coincidence gates on the 574- and 663-keV transitions, individually shown in Fig. 4. In such a spectrum the intensity of the 330-keV γ ray would have to balance that of the sum of the 505- and the 791-keV
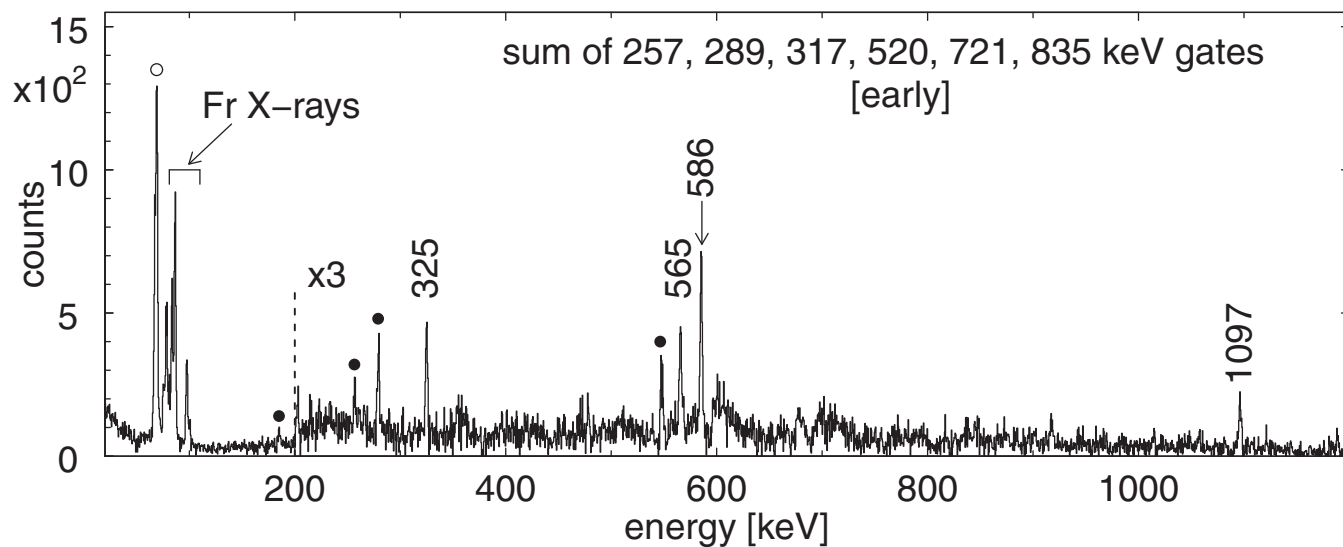
FIG. 5. Sum of early ($\Delta T = 150$–856 ns) γ-ray coincidence spectra for the 257-, 289-, 520-, 721-, and 835-keV transitions. Solid and open circles have the same meaning as in Fig. 2.

lines, with the difference in observed intensities owing to conversion. Similar analyses have been conducted to derive total conversion coefficients for the lines at 64, 119, 143, 204, 257, 271, 286, 317, 330, and 520 keV. Measurements for higher energy lines such as the the 574- and 663-keV transitions become marginal. The results are presented in Table II and in Fig. 6.

D. Lifetimes and transition strengths

The lifetimes of four states in ^{210}Fr have been determined by combining, in some cases, values from complementary sources. For example, the meanlife of the isomer at 1113 keV was obtained first from the time dependence of the γ-γ coincidence intensity of the 817- and 271-keV transitions in the chopped experiment data (Fig. 7). Then a second measurement was extracted from the time-difference data in the pulsed beam experiment, obtained with gates on the 529-keV transition that directly feeds the 1113-keV state and on the 817-keV transition. (Having determined that the intermediate state at

842 keV does not have a significant lifetime, use of the 817-keV line rather than the 271-keV transition that directly populates the state results in an improved timing response.) The resultant spectrum in Fig. 8 is fitted with a decay curve convoluted with the prompt response function. A combination of the two measurements gives the adopted lifetime of $\tau = 29.8(7)$ ns.

The lifetime of $\tau = 8(2)$ ns for the isomer at 2018 keV was extracted from a fit to the spectrum in Fig. 9, obtained with a gate on the 1176-keV line in the time-γ measurement with the nanosecond pulsed beam and confirmed (with less precision) from the γ-γ time data.

The mean life of the isomer at 2206 keV is short and was determined largely from a generalized centroid shift analysis of γ-γ time difference spectra. A lifetime of 1.79(11) ns was deduced from the time-γ-γ coincidence spectra produced with one gate on the 817- or 257-keV, transition and the other on transitions above the isomer at 2206 keV, such as the 835- or
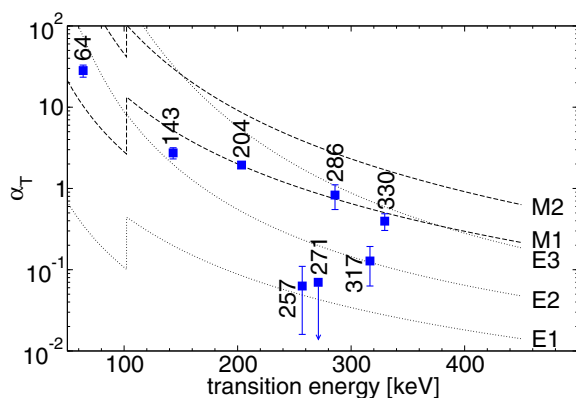

FIG. 6. Comparison of total conversion coefficients deduced from intensity balances for selected transitions in ^{210}Fr with calculated values for pure transitions from Ref. [25].
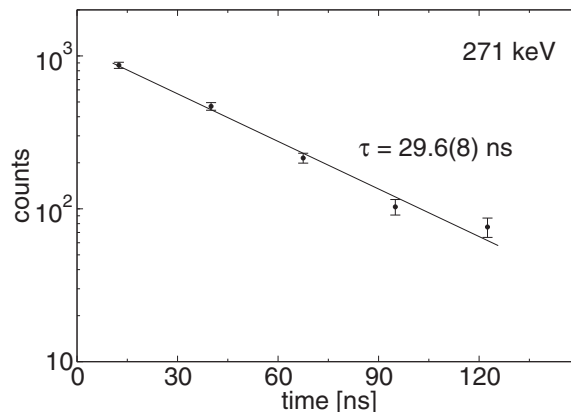

FIG. 7. Intensity of the 271-keV transition observed in coincidence with the 817-keV transition in various out-of-beam time regions in the $1/9$-μs chopped-beam experiment. A lifetime of 29.6(8) ns is deduced.

TABLE II. Total conversion coefficients for selected transitions in ^{210}Fr, deduced from intensity balances.

E_γ	Exp.	Assignment	Theory[a]				
			$E1$	$M1$	$E2$	$M2$	$E3$
63.9	28(5)	$M1 + E2$	0.355	10.4	74.1	319	3051
118.9	9.8(6)	$M1$	0.311	8.75	4.27	59.2	90.0
143.2	2.7(4)	$M1$	0.198	5.16	1.98	30.0	32.7
203.5	1.94(15)	$M1$	0.0846	1.91	0.520	8.61	5.31
256.9	0.06(5)	$E1$	0.0488	0.998	0.235	3.88	1.75
271.0	<0.07	$E1$	0.0431	0.861	0.198	3.24	1.37
285.8	0.8(3)	$M1$	0.0382	0.744	0.168	2.71	1.09
316.6	0.13(7)	$E2$	0.0303	0.562	0.123	1.94	0.701
329.6	0.40(9)	$M1 + E2$	0.0277	0.503	0.110	1.70	0.594
396.6	0.25(4)	$M1$[b]	0.0185	0.304	0.0658	0.938	0.291
396.6	0.38(5)	$M1$[c]	0.0185	0.304	0.0658	0.938	0.291
486.4	0.23(4)	$M1$[d]	0.0121	0.176	0.0394	0.498	0.143
486.4	0.44(6)	$M1$[e]	0.0121	0.176	0.0394	0.498	0.143
519.6	0.19(7)	$M1$	0.0105	0.147	0.0337	0.408	0.116

[a]Calculated values from Ref. [25].
[b]Assuming an $E3$ assignment for the 663.3-keV transition.
[c]Assuming an $M2$ assignment for the 663.3-keV transition.
[d]Assuming an $E3$ assignment for the 573.5-keV transition.
[e]Assuming an $M2$ assignment for the 573.5-keV transition.

the 330-keV γ rays directly feeding it. Various estimates of the energy-dependent prompt response function necessary for this analysis were available from intense cascades through short-lived states with similar transition energies found in other reaction products in the same data set. For example, the 817-keV transition in ^{210}Fr, the 820- and 800-keV transitions in ^{211}Fr [8], and the 818-keV transition in ^{210}Rn were used in conjunction with a range of coincident γ-rays.

Finally, the lifetime for the isomer at 4417 keV was measured using the time-γ-γ coincidence data from the microsecond chopped-beam experiment. A mean life of 686(9) ns was deduced from a fit to the decay curve displayed in Fig. 10. The spectrum was constructed by combining the coincidence intensities of a range of transitions in coincidence with either the 574- or 663-keV branches from the isomer,

in a sequence of contiguous time regions. Note that the same technique gave a lifetime of $\tau = 179.6(17)$ ns for the 4657-keV isomer in ^{211}Fr (see Fig. 11), in good agreement with the value reported by Byrne *et al.* of $\tau = 178(20)$ ns [8].

The transition strengths for branches from the identified isomers, including limits on the decays from the 1627 keV 12^+ state, are presented in Table III.

E. Spin and parity assignments

Spin and parity assignments were made through a consideration of the total conversion coefficients, anisotropies, and transition strengths (measured and implied), as well as the occurrence or absence of branches to lower states.
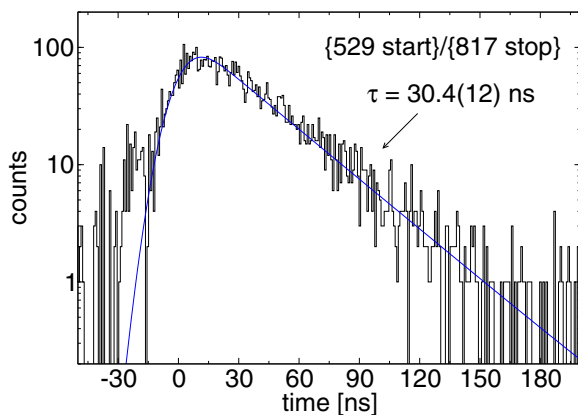

FIG. 8. Time spectrum obtained by measuring the time difference between the 529- and the 817-keV transitions in the 1/1712-ns pulsed beam experiment. The measured mean life is 30.4(12) ns.
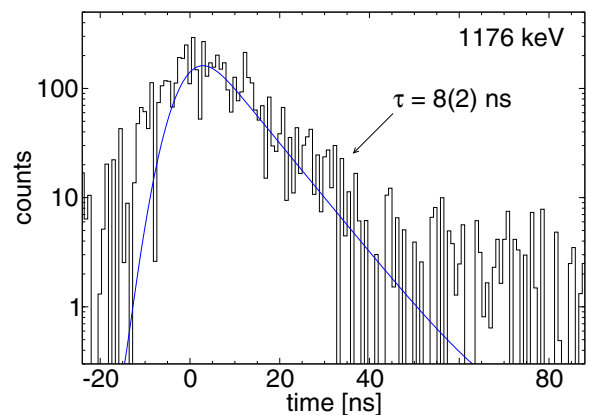

FIG. 9. Time spectrum relative to the beam pulse, obtained from the 1/1712-ns pulsing experiment with a gate on the 1176-keV transition. The deduced lifetime for the state at 2018 keV is 8(2) ns.
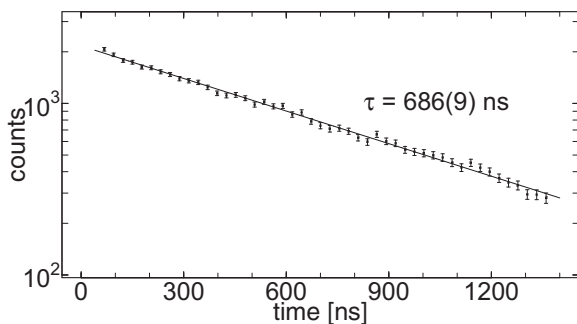
FIG. 10. Time behavior of coincidence intensities for transitions below the 4417-keV isomer, in the $1/9$-μs chopped-beam experiment. A lifetime of 686(9) ns is deduced for the 4417-keV state.

The ground-state spin and parity of 6^+ was measured by Ekström *et al.* [26] through on-line atomic beam magnetic resonance techniques. The 817- and 721-keV γ rays that form the main cascade at low spins and feed the proposed 7^+, 24.8-keV excited state, have anisotropies of $+0.28(2)$ and $+0.27(3)$, respectively. (The angular distribution for the intensity of the 721-keV transition in spectra gated on the 817-keV line, for the pairs of detectors at $\pm34.75°$, $\pm48.75°$, and $\pm82.75°$, is shown in Fig. 12.) These are characteristic of stretched $E2$ transitions (alternative $M2$ assignments would imply measurable longer lifetimes) and suggest $J^\pi = 9^+$ and 11^+ for the 842- and 1563-keV states, respectively. Similar anisotropies are observed for the 793- and 289-keV γ rays, while the value for the 225-keV branch from the 1563-keV state of $A_2 = -0.21(4)$ is consistent with a stretched $M1$
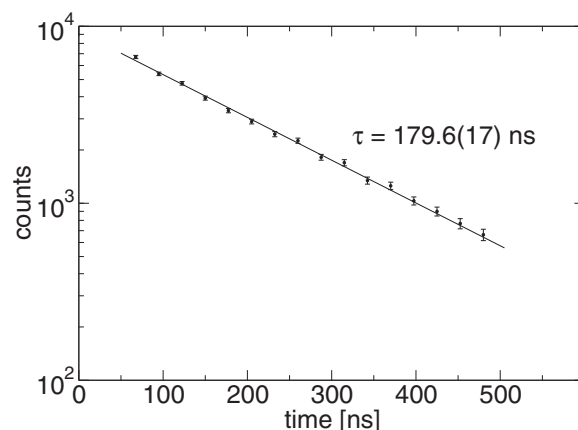

FIG. 11. Measurement of the lifetime of the isomeric state at 4657 keV in ^{211}Fr obtained by adding the coincidence intensities for several transitions, observed in the $1/9$-μs chopped-beam experiment.

multipolarity. Taken together, these observations imply $J^\pi = 10^+$ for the 1337-keV state, $J^\pi = 8^+$ for the 544-keV state populated by the 793-keV transition, and $J^\pi = 12^+$ for the 1627-keV state that decays via the 289-keV transition.

The 520-keV transition from the 8^+, 544-keV state to the 25-keV state is a dipole transition with a total conversion coefficient that suggests $M1$ multipolarity, although the large negative distribution coefficient of $A_2 = -0.44(3)$ implies a significant $E2$ admixture. This is consistent with the assumed $J^\pi = 7^+$ for the 25-keV state. In contrast, the

TABLE III. γ-ray branching ratios and transition strengths for selected states in ^{210}Fr.

Initial state, τ	Final state, J^π	E_γ (keV)	I_γ	$\sigma\lambda$	α_T [a]	$B(\sigma\lambda)$ (e^2 fm$^{2\lambda}$ or μ_0 fm$^{2(\lambda-1)}$)	Transition strength (W.u.)
$(23)^+$ 4417 keV							
686(9) ns	20^-	663.3	52.4(14)	$(E3)$[b]	0.0569	$2.21(8) \times 10^4$	8.4(3)
	20^-	573.5	47.6(12)	$(E3)$[b]	0.0861	$5.56(19) \times 10^4$	21.2(7)
15^- 2206 keV							
1.79(11) ns	14^+	256.9	100	$E1$	0.04881	$1.98(14) \times 10^{-5}$	$8.7(7) \times 10^{-6}$
12^+ 1627 keV							
<1.5 ns	10^+	289.1	1000(40)	$E2$	0.1620	>61	>0.82
	11^+	63.8	152(20)	$M1$	9.9(11)	>0.005	>0.003
	11^+	36.5	*20(3)*	$M1$	53.84	>0.003	>0.002
11^- 2018 keV							
8(2) ns	9^+	1176.3	92(4)	$M2$	0.04053	2.1(6)	$3.7(10) \times 10^{-2}$
	11^-	376.7	8(4)	$M1$	0.351	$6(3) \times 10^{-6}$	$3(2) \times 10^{-6}$
	11^-	346.2	12(5)	$M1$	0.440	$1.2(6) \times 10^{-5}$	$7(3) \times 10^{-6}$
	11^-	17.2[c,d]	0.42	$M1$	123.6	$3.4(9) \times 10^{-3}$	$1.9(5) \times 10^{-3}$
10^- 1113 keV							
29.8(7) ns	9^+	271.0	100	$E1$	0.0431	$1.01(3) \times 10^{-6}$	$4.5(2) \times 10^{-7}$

[a]Calculated values, from Ref. [25].

[b]Assuming the 4417-keV state is $(23)^+$. The alternative $(22)^+$ assignment with $M2$ decays is discussed below.

[c]Values estimated from $I_\gamma(888.1 \text{ keV}) = 51(4)$, $\sigma\lambda(888.1 \text{ keV}) = M1$, and $\alpha_T(888.1 \text{ keV}) = 0.0358$. Note that the strengths of the three parallel transitions were calculated using the 888.1-keV γ ray, hence assuming 100% intensity balance between the 17.2- and 888.1-keV transitions.

[d]Note that if the transition were to contain an $E2$ component, as possible for $J \to J$ transitions, then the conversion coefficient would be much higher $[\alpha_T(17.2 \text{ keV}, E2) = 29\,490]$.
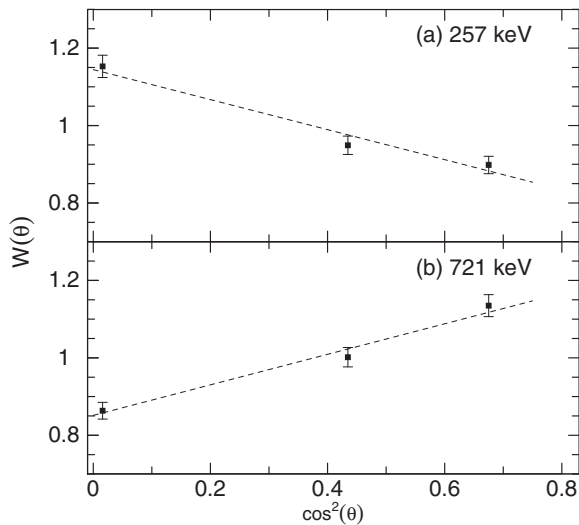
FIG. 12. Angular distributions for the (a) 257-keV and (b) 721-keV transitions. These are gated angular distributions where the gating transition (817 keV for these two cases) was observed at any of the six angles in CAESAR, while the three data points correspond to the measured intensities for pairs of detectors at $\pm 34.75°$, $\pm 48.75°$, and $\pm 82.75°$. The intensity data were fitted with a Legendre polynomial expansion, $W(\theta) = A_0 + A_2 P_2[\cos(\theta)]$, and is normalized in the figure by the fitted value of A_0, with the best-fit values of A_2/A_0 shown. Because these are gated distributions, the values of A_2/A_0 may be slightly perturbed from the values that would be observed in singles measurements. The expected perturbations have been calculated to be small for the detector angles in CAESAR.

544-keV branch direct to the ground state has a positive A_2 coefficient [$+0.40(3)$] consistent with a stretched $E2$ transition and the known 6^+ spin and parity of the ground state, although the anisotropy is a little larger than expected. Similar considerations for the 903-keV transition lead to $J^\pi = 10^+$ for the 1447-keV state that also decays via the 693- and 754-keV cascade through the 754-keV state, assigned as $J^\pi = 8^+$ with a stretched 754-keV $E2$ transition, leading again, with consistent multipolarities, to the 6^+ ground state. We note that the 754-keV state has the same properties as that reported by Kuusiniemi *et al.* [23]; however, if they are the same states, it is somewhat surprising that (a) we do not see the 139-keV state seen by them in Ref. [23] and (b) they did not observe our 544-keV state (also 8^+ and lower in energy than the 754-keV state) in their α-decay study.

The anisotropy and total conversion coefficient for the 143-keV line that feeds the 1447-keV state both suggest a mixed $M1/E2$ multipolarity, giving 11^+ for the state at 1592 keV. This implies that the unobserved 36.5-keV transition from the 1627-keV state is an $M1$, with the upper limit on the 1627-keV state mean life giving an acceptable strength of >0.002 W.u. (see Table III).

The total conversion coefficient for the 64-keV transition that connects the 1627- and 1563-keV states suggests a mixed $M1/E2$ character, consistent with the lifetime limit of $\tau < 1.5$ ns (Table III) for the 12^+ state at 1627 keV. The multipolarity of the 64-keV transition is also consistent with the assignment for the 289- and 225-keV γ rays discussed above. The transition-

strength limit for the 289-keV $12^+ \rightarrow 10^+$ transition of >0.82 W.u. can be viewed in the context of the strength of the 233-keV $E2$ decay of the 3.0(3)-ns, 1686-keV state in ^{211}Fr. This $21/2^- \rightarrow 17/2^-$ transition within the $\pi h_{9/2}^5$ core multiplet has a strength of 4.0(4) W.u. [8], the difference in lifetime being largely attributable to the E_γ^5 factor.

Proceeding to the higher states in this sequence, the conversion coefficients for the 118.9-, 203.5-, and 256.9-keV transitions imply assignments of $M1$, $M1$, and $E1$ multipolarities, respectively, while the angular distribution results suggest stretched dipole character for the 256.9-keV γ ray. The latter distribution, from spectra gated on the 817-keV line, is shown in Fig. 12. This leads to assignments of 13^+, 14^+, and 15^- for the 1746-, 1949-, and 2206-keV states, respectively.

Higher in the scheme, the total conversion taken together with anisotropies, suggests that the 330-keV γ ray is a mixed $M1/E2$ transition giving $J^\pi = 16^-$ for the 2536-keV state. The 835-keV γ ray that feeds most of the intensity to the 15^- state at 2206 keV is assigned as a stretched $E2$ transition from the measured angular distribution coefficient of $A_2 = +0.36(3)$, giving $J^\pi = 17^-$ for the 3041-keV state. The parallel 505.2-keV transition has a large negative anisotropy, suggesting a mixed $M1/E2$ multipolarity and a $\Delta J = 1$ character, independently leading to $J^\pi = 16^-$ for the 2536-keV state.

The 3327-keV state has a 285.8-keV, $M1$ stretched dipole decay [$A_2 = -0.35(2)$ and $\alpha_T = 0.8(3)$] to the 3041-keV, 17^- state and a 791.0-keV stretched quadrupole [$A_2 = 0.25(10)$] branch to the 2536-keV, 16^- state, justifying a $J^\pi = 18^-$ assignment. The main decay of the 3357-keV state, which also has an unobserved 30.8-keV branch to the 3327-keV state, is via the stretched $E2$, 317-keV transition [$A_2 = 0.34(3)$ and $\alpha_T = 0.13(7)$] to the 3041-keV state; hence the 19^- assignment.

The 3357-keV, 19^- state is directly fed by the 396.6- and the 486.4-keV transitions that have $A_2 = -0.28(3)$ and $-0.34(4)$, respectively, both suggestive of stretched-dipole or mixed dipole/quadrupole character. Ignoring the non-dipole possibilities, the internal conversion coefficients for both lines clearly favor $M1$ character over $E1$ (see Table II), irrespective of the multipolarity assignments for the two γ rays at 573.5 and 663.3 keV. Hence, the 3754- and 3844-keV states can both be assigned $J^\pi = 20^-$.

The 4417-keV state has two branches of similar intensity, with energies of 573.5 and 663.3 keV. These are too high in energy to be able to extract reliable total conversion coefficients, especially in the case of the 663-keV transition. However, we note that the conversion coefficients for the daughter transitions at 486.4- and 396.6-keV, respectively, are both in better agreement with their $M1$ assignments, if the higher transitions are $E3$. It is also worth noting that mismatching assignments for the 573.5- and 663.3-keV γ rays would imply that one of the 486.4- and 396.6-keV transitions is a $J \rightarrow J$, mixed $M1/E2$ transition, for which the conversion coefficient would be lower than what is reported in Table II.

The 573.5- and 663.6-keV γ rays have large anisotropies of $+0.35(7)$ and $+0.41(6)$, respectively, suggesting they are either stretched quadrupoles, or more likely, given the long lifetime and the fact that there should be significant
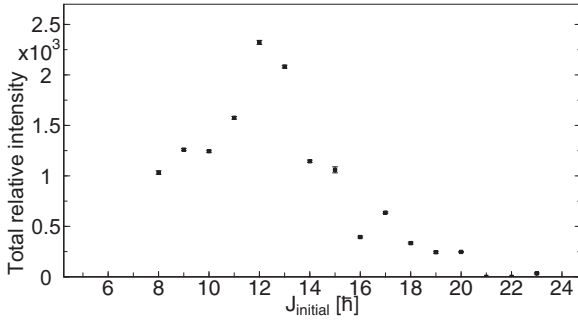
FIG. 13. Relative intensities for total transition intensity decaying from states with spin J_{initial}. Note that the depletion of intensity at high ℓ is most likely a result of fission competition, while at low ℓ, it is an artifact of the high fragmentation of the level scheme that produces almost equally populated even- and odd-spin states.

spin deorientation, stretched octupoles. Consideration of the transition strengths leads to the interim conclusion that both are probably of $E3$ character. This leads to the tentative assignment of $J^{\pi} = (23)^{+}$ for the 4417-keV isomeric state.

Note that the population of the isomer is relatively low given its yrast nature and the angular momentum input in the reaction used, but this is probably a result of the fission competition that sets in for these more neutron-deficient cases, severely depleting evaporation residues with high-ℓ values; see Fig. 13.

There are several transitions that feed into the 3754- and 3844-keV states (both 20^{-}) but bypass the isomer at 4417 keV. Of these, the angular distributions suggest that both the 250.7- and 340.2-keV γ-ray branches from the 4094-keV state are dipoles, and the absence of a branch to the 19^{-} state (an $E2$ in the case of negative parity) would suggest $J^{\pi} = 21^{+}$. However, the absence of what would be a 323-keV, $E2$ branch to this state from the 4417-keV isomer results in the $(21)^{-}$ assignment.

The levels placed on the right-hand side of Fig. 1 are now considered. The strong 271.0-keV γ ray feeding the 842-keV 9^{+} state is a dipole transition $[A_2 = -0.13(4)]$, with a limit on the conversion coefficient of $\alpha_T \leqslant 0.07$ that implies $E1$ multipolarity and hence $J^{\pi} = 10^{-}$ for the 1113-keV isomeric state. The strength of 4.5×10^{-7} W.u. for the 271.0-keV transition (see Table III) is consistent with that measured for similar $E1$ transitions in the neighboring nuclei. The 888.1-keV γ ray that feeds the 10^{-} state is probably a mixed dipole/quadrupole $[A_2 = 0.77(27)]$. An $M2$ component is unlikely given the absence of a significant lifetime [for $B(M2) < 1$ W.u., $\tau > 10$ ns], so it must be of mixed $M1/E2$ multipolarity, giving $J^{\pi} = 11^{-}$ for the 2001-keV state.

There is a weak, unobserved 17.2-keV branch to the 2001-keV state from the 8-ns isomer at 2018 keV, established by the crossover transitions. The main branch is the 1176-keV γ ray to the 9^{+}, 842-keV state with an angular distribution that suggests a stretched quadrupole and therefore either $J^{\pi} = 11^{+}$ or 11^{-}. An $E2$ assignment would not result in a measurable lifetime, whereas an $M2$ assignment gives a plausible strength of $6(1) \times 10^{-3}$ W.u.; see Table III. Hence, negative parity has been suggested in the level scheme.

The cascade of 280.4-, 325.5-, and 365.5-keV transitions above are all dipoles, possibly of $M1$ multipolarity although $E1$ cannot be excluded. This is the basis for assignments of (12^{-}), (13^{-}), and (14^{-}) for the 2298-, 2624-, and 2989-keV states, respectively, with $J^{\pi} = (15^{-})$ suggested for the 3103-keV state.

The 3129-keV state has two unobserved low-energy branches to the 3118- and 3103-keV state but no transition to the 2989-keV proposed 14^{-} state. Its main branch is the 923.2-keV dipole transition $[A_2 = -0.33(3)]$ and from this we propose an assignment of $J^{\pi} = 16^{(-)}$. Finally, the cascade transitions above are all dipoles (see Table I) and none of the states have a significant lifetime, leading to suggested spins and parities of $17^{(-)}$, $18^{(-)}$, and $19^{(-)}$ for the 3520-, 3812-, and 3975-keV states, respectively.

IV. DISCUSSION

A. Background

The semiempirical shell model has been highly successful in describing nuclei in the lead region [7]. Most of the levels observed in ^{210}Fr owe their origin to the coupling of the five valence protons in the $\pi[h_{9/2}, f_{7/2}, i_{13/2}]^{5}$ space with the three neutron-holes in the $\nu[p_{1/2}, f_{5/2}]^{-3}$ space. With such a high number of valence particles and available shells it is expected that calculations will not be able to reproduce the experimental states very well. Consequently, the interpretation of the level scheme is not straightforward.

Owing to the availability of high-angular-momentum orbits (e.g., the highest member of the $\pi h_{9/2}^{3} i_{13/2}^{2} \nu f_{5/2}^{-1} i_{13/2}^{-2}$ multiplet has an angular momentum of $37\hbar$), the high-spin levels in the present case are expected to be formed by excitation of the valence protons and neutron-holes rather than core excitation; the latter possibility is more likely for nuclei nearer to the $N = 126$ shell closure (see, for example, Refs. [7,8]).

The studies of the astatine isotopes, such as ^{208}At by Fant *et al.* [27], showed a division of the level scheme between proton and neutron-hole excitations. Such separation in the system ^{210}Fr can be seen from the perspective of a coupling of its two cores, $|^{205}\text{Pb} \otimes ^{213}\text{Fr}\rangle$. This would result in analogous states for purely proton or neutron-hole excitations, with similar energies observed in ^{210}Fr relative to the relevant core nuclei. As shown later, good examples are the relatively constant energy at which (a) the 10^{-} isomer is observed in any of the bismuth, astatine, or francium even-isotope series and (b) the high-spin long-lived isomer is observed in the $209 \leqslant A \leqslant 213$ francium isotopes; see Fig. 14. Another consequence of the superposition of the two cores is that the shell-model calculation for ^{210}Fr principally relies on the accuracy of such calculations for ^{205}Pb and ^{213}Fr. For the latter nucleus, calculations were presented by Byrne *et al.* [8], and, while calculations were performed anew for this work with up-to-date two-body interactions from Bayer *et al.* [3], no significant changes were observed. Maximal spins for non-core-excited states are obtained with the $\pi h_{9/2}^{3} i_{13/2}^{2}$ $(J^{\pi} = 45/2^{-})$ and $\pi h_{9/2}^{2} i_{13/2}^{3}$ $(J^{\pi} = 49/2^{+})$ configurations.

A comparison of experimental and calculated states for ^{205}Pb is shown in Fig. 15. Neutron-holes can also contribute for a substantial amount of angular momentum, with, for
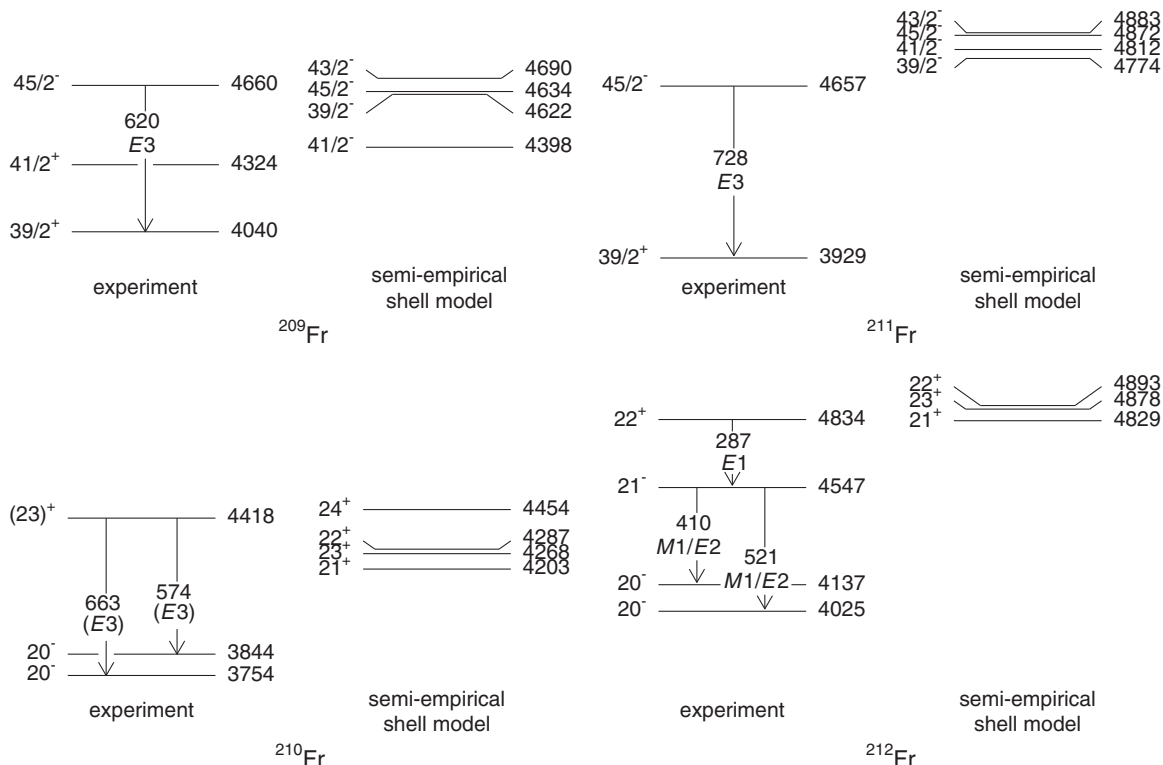
FIG. 14. Comparison of the decay of the high isomer in the $209 \leqslant A \leqslant 213$ francium isotopes.

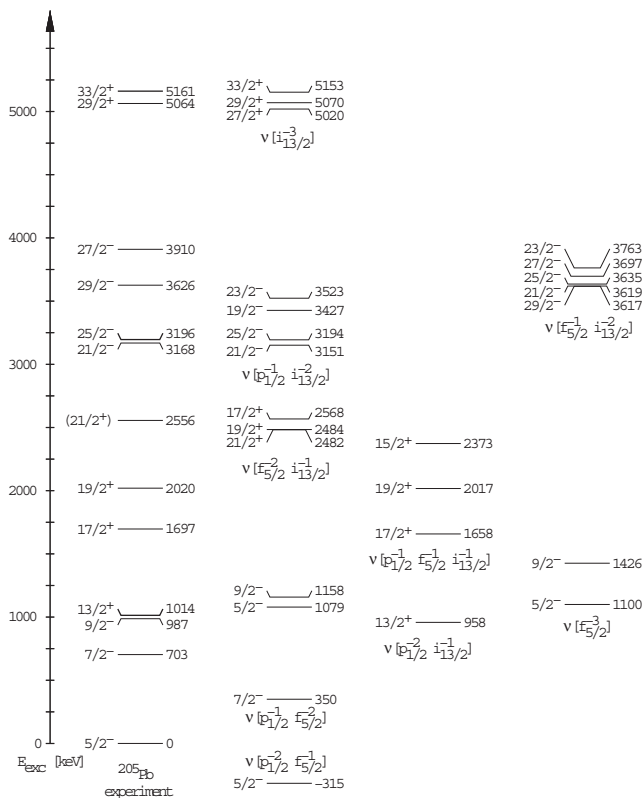

FIG. 15. Comparison between the calculated (present work) and experimentally measured levels in ^{205}Pb.

example, and as suggested by the levels of the neutron core excitation, several $J = 21/2$ states available below $\sim$3 MeV.

In Fig. 16, the result of calculations for states within the configuration space for ^{210}Fr is compared to the observed scheme. The overall agreement is worse than that reported by Byrne *et al.* [8] for the three next heavier isotopes. While, typically, accuracy up to 150 keV can be observed in $^{211-213}$Fr for pure configurations [8], far worse agreements are found here. With increasing number of valence nucleons, it is expected that mixing of different configurations may occur. Blomqvist *et al.* [28] have developed another method to perform shell-model analysis of particular states in a nucleus based upon the observation of the assumed corresponding configurations in nearby nuclei. Poletti *et al.* [29] have shown an application in the case of ^{209}Rn. In this method, mixing of configurations is taken into account if similar mixing is present in the nuclei used in the state decomposition. The 19^- state in ^{210}Fr was successfully described following this procedure, with an inferred energy of 3395 keV, 38 keV from the observed energy of 3357 keV (see Ref. [24], or Ref. [29] for an application to ^{209}Rn). This can be compared with the pure configuration calculation, shown in Fig. 16, that predicts 19^- states at 3011 and 3574 keV, 346 and 217 keV away from the observed state, respectively.

B. Configuration assignment

As expected from the above explanation, an overall view of the level scheme presented in Fig. 1 shows a division into two

FIG. 16. Comparison between the calculated and experimentally measured levels in ^{210}Fr. Experimental states are split left and right, similar to the level scheme in Fig. 1.

parts. The right-hand side levels can mainly be explained by the $\nu i_{13/2}^{-1}$ excitation, whereas the left-hand side contains states resulting from the $\pi h_{9/2}^5$ or $\pi h_{9/2}^4 f_{7/2}$ excitations. Also, this side of the level scheme has higher level density owing to the similarity of the $\langle \pi h_{9/2}|\nu(p_{1/2}, f_{5/2})^{-1}\rangle$ two-body interaction energies (see Refs. [2,3]), with the first consequence being the closeness of the 6^+ ground state and the 7^+ first excited state. A somewhat comparable situation was seen in, for example, the isotone ^{208}At [27].

The ground state is believed to be the $J^\pi = 6^+$ member of the $\pi(h_{9/2}^5) \otimes \nu(p_{1/2}^{-2}f_{5/2}^{-1})$ multiplet. Within this multiplet the energy difference between the 6^+ and 7^+ is well reproduced by the calculation ($\Delta_{\mathrm{exp}} = 25$ keV and $\Delta_{\mathrm{calc}} = -12$ keV); see Fig. 16. (Note that the discrepancy between experiment and calculation for the ground state, ≈ -330 keV, is very similar to that observed in ^{205}Pb, suggesting this is driven by the neutron-hole behavior.) In the left-hand side, states below the 1626-keV excitation can be mostly explained by the same multiplet as the ground state, although there are unclear cases where one of the protons could be in the $f_{7/2}$ orbital rather than $h_{9/2}$.

At low spins, the observation of two 8^+ and two 10^+ states exemplifies the competition between either the two different neutron-hole configurations, $\nu(p_{1/2}^{-2}f_{5/2}^{-1})$ and $\nu(p_{1/2}^{-1}f_{5/2}^{-2})$, or different recoupling within the same multiplet. Again, there is a lack of clear guidance from the calculation. However, the similar energy of the 11^+ state in ^{210}Fr, $E_x^{1^{st}} = 1563$ keV and in ^{212}Fr, $E_x = 1555$ keV [8] suggests that the structure proposed by Byrne *et al.*, $\pi(h_{9/2}^5) \otimes \nu(p_{1/2}^{-1})$ persists in ^{210}Fr, with the inclusion of two passive, extra holes in the $\nu f_{5/2}$ orbital. Furthermore, while the 11^+ state was an isomer in the heaviest of these two isotopes, the decaying γ-ray energy changes in ^{212}Fr, compared to ^{210}Fr, from 162 to 721 keV, respectively, and reduces the lifetime below detection limits. Note also that the $11^+ \rightarrow 9^+$ energy gap is very similar in ^{210}Fr and ^{208}Fr [16] (721 and 724 keV, respectively), where no lifetime is seen in either case.

The assignment for levels leading to the state at 1949 keV with $J^\pi = 14^+$ is uncertain. This is attributable to the lack of clear guidance from the calculation; see Fig. 16. Nevertheless, the $12^+ \rightarrow 10^+$, 289-keV, $E2$ transition has an implied strength in agreement with the $21/2^- \rightarrow 17/2^-$, 233-keV, $E2$ transition in ^{211}Fr, as noted before, and the $17/2^- \rightarrow 13/2^-$, 222-keV, $E2$ transition in ^{213}Fr [8]. The transition energy difference is sufficient to explain why the 12^+ state in ^{210}Fr does not have a lifetime. Consequently, it is suggested that all positive states from the ground state to the 1949-keV, $J^\pi = 14^+$ state, are from excitations of $\pi(h_{9/2}^5)$ coupled to the neutron-holes aligned to either $3/2^-$ or $1/2^-$ (due to the strongly repulsive proton-neutron-hole interaction). The 15^- to 12^+ energy gap in ^{210}Fr is similar to that in ^{212}Fr (580 keV compared to 612 keV); however, unlike ^{212}Fr, the isomer decays by an $E1$ transition due to the much lower energy of the 14^+ state in ^{210}Fr, thus favoring the $E1$ branch over the possible $E3$ transition. A 563-keV, $E3$ transition ($29/2^+ \rightarrow 23/2^-$) is also observed in ^{211}Fr, but again the energy gap with the $27/2^-$ state is smaller than the 15^- to 12^+ energy gap in ^{210}Fr, therefore not favoring

the $E1$ decay. The 15^- isomer is more likely a member of the $\pi(h_{9/2}^4 i_{13/2}) \otimes \nu(p_{1/2}^{-2}f_{5/2}^{-1})$ multiplet. The yrast sequence up to the 19^- state at 3357 keV is very likely attributable to the same configuration.

1. Configuration of the isomer at $E_x = 4417$ keV

At 4417 keV a 686(9)-ns isomer has been discovered. It decays via two most likely $E3$ transitions at 573.5 and 663.3 keV. This is supported by the angular distribution for those transitions $+0.35(7)$ and $+0.41(6)$, respectively, although the presence of residual alignment with a state of this lifetime is surprising and suggests that the hyperfine interaction between gold and francium is small. Note that we also measured the A_2/A_0 for the 728-keV, $E3$ decay of the $49/2^-$, 178-ns isomer in ^{211}Fr at $+0.27(4)$, very similar to the value obtained (using a molten target) by Byrne *et al.* [8]. The agreement between the two measurements further supports the angular distributions reported for the 573.5- and 663.3-keV γ rays. Total internal conversion coefficients for the subsequent transitions are also in favor of an $E3$ assignment. However, an $M2$ assignment cannot be strictly rejected, especially for the transition at 573.5 keV.

Long-lived high-spin isomers ($J^\pi = 45/2^-$) have been measured in ^{209}Fr by Dracoulis *et al.* [15] and ^{211}Fr by Byrne *et al.* [8]. The states have been assigned as members of the $\pi(h_{9/2}^3 i_{13/2}^2) \otimes \nu(p_{1/2}^{-2}f_{5/2}^{-2})$ and $\pi(h_{9/2}^3 i_{13/2}^2) \otimes \nu(j^{-2})$ multiplet, respectively, in which the neutron-hole pairs are coupled to zero angular momentum. In ^{210}Fr, a similar state is expected to occur from the $\pi(h_{9/2}^3 i_{13/2}^2) \otimes \nu(p_{1/2}^{-2}f_{5/2}^{-1})$ configuration, which can yield a maximum spin (and parity) of 25^+. However, the residual interaction between protons and the odd neutron hole does not favor mutual alignment and the isomer from that configuration is expected at lower spin. The 23^+ state is a potential candidate, however, according to the calculations in Fig. 16, there could be a competitive $E2$ γ ray to a lower 21^+ state. This is not observed, but neither were the analogous transitions in the neighboring isotopes (see Ref. [19] and Fig. 14).

The transition strengths for the two transitions decaying from the isomer at 4417 keV are reported in Table IV for several scenarios. The transition strength for the 573.5-keV γ-ray in case of an $E3$ assignment is consistent with the typical values, around 22 W.u. [30], that are obtained in the case of a $\tilde{i}_{13/2} \rightarrow \tilde{f}_{7/2}$ transition, where the tildes signify that those are empirical state configurations rather than pure single particles. This would mean that the final-state configuration is $[\pi(h_{9/2}^3 i_{13/2} f_{7/2}) \otimes \nu(p_{1/2}^{-2}f_{5/2}^{-1})]_{20^-}$. The transition strength for a possible 663-keV $E3$ γ-ray, 8.4 W.u., is too low to be explained by the argument developed for the case of a 574-keV $E3$ transition. A slower transition could be explained by lower admixtures of the collective 3^- phonon. Such should be the case for both transitions if those were from the same multiplet; hence the possibility of a spin-flip transition to the 20^- member of the $\pi(h_{9/2}^4 i_{13/2}) \otimes \nu(p_{1/2}^{-2}f_{5/2}^{-1})$ multiplet. (Note that this would still be $\tilde{i}_{13/2} \rightarrow \tilde{h}_{9/2}$.) However, in their $B(E3)$ systematics study, Bergström and Fant [30] reported an average value of 3 W.u. for such transitions, clearly too low compared to what we measured. The empirical shell-model

TABLE IV. Branching ratios and transition strengths for the decay of the $(23)^+$ isomer in ^{210}Fr and comparison with neighboring odd Fr isotopes. Various spin assignments for the 3754- and 3844-keV states are considered.

Nucleus state	Initial state, τ	Final state, J^π	E_γ (keV)	I_γ	$\sigma\lambda$	α_T[a]	Transition strength (W.u.)
^{210}Fr	$(23)^+$ 4417 keV						
	686(9) ns	$(20)^-$	663.3	52.4(14)	$E3$	0.0569	8.4(3)
		$(20)^-$	573.5	47.6(12)	$E3$	0.0861	21.2(7)
	$(23)^+$ 4417 keV						
	686(9) ns	$(21)^-$	663.3	52.4(14)	$M2$	0.1980	$6.1(3) \times 10^{-3}$
		$(21)^-$	573.5	47.6(12)	$M2$	0.3033	$1.12(4) \times 10^{-2}$
	$(23)^+$ 4417 keV						
	686(9) ns	$(21)^-$	663.3	52.4(14)	$M2$	0.1980	$6.6(3) \times 10^{-3}$
		$(20)^-$	573.5	47.6(12)	$E3$	0.0861	19.8(7)
^{211}Fr	$45/2^-$ 4657 keV						
	178(20) ns	$39/2^+$	728.3	100(1)	$E3$	0.045	33(4)
^{209}Fr	$45/2^-$ 4660 keV						
	606(26) ns	$39/2^+$	620.2	100.0(2)	$E3$	0.0686	28.8(12)
		$41/2^+$	335.5	1.1(2)	$M2$	1.602	$4.9(9) \times 10^{-3}$

[a]Total conversion coefficients are taken from Ref. [25].

calculation of Fig. 16, however, reproduces quite well the energy between the two final states in the case of a $\tilde{i}_{13/2} \to \tilde{f}_{7/2}$ transition and a spin-flip transition. Two states from the same multiplet seems highly unlikely for the 20^- assignments. Mixing of different configurations has also been considered and is, in fact, very likely to be involved in the final states, because enough 20^- states are predicted in the semiempirical calculation of Fig. 16 to support such an explanation. However, given the remaining uncertainty regarding the multipolarity of the 573.5- and 663.6-keV γ rays, further speculation is not appropriate.

Alternatively, the isomer could be the 22^+ member of the $\pi(h_{9/2}^3 i_{13/2}^2) \otimes \nu(p_{1/2}^{-2} f_{5/2}^{-1})$ multiplet and thus, if the $E3$ assignments hold, the two final states would be the two lower 19^- states of the $\pi(h_{9/2}^3 i_{13/2} f_{7/2}) \otimes \nu(p_{1/2}^{-2} f_{5/2}^{-1})$ multiplet. However, because of the firm 20^- assignment for the two states at 3754 and 3844 keV, $J^\pi = 22^+$ for the isomer would lead to $M2$ assignments for both transitions at 574 and 663 keV. This would also result in a significant lifetime. Considering the possible configuration changes, the implied $M2$ strength of $\sim$0.006 W.u. for the 663.3 keV γ ray (see Table IV) is consistent with a j-forbidden $M2$ transition [15]. A possibility then is that the state at 3754 keV is a member of the $\pi(h_{9/2}^3 i_{13/2} f_{7/2}) \otimes \nu(p_{1/2}^{-2} f_{5/2}^{-1})$ multiplet ($\Delta \ell = 4$ for the transition) but it could not be from the $\pi(h_{9/2}^4 i_{13/2}) \otimes \nu(p_{1/2}^{-2} f_{5/2}^{-1})$ multiplet because an $M2$ transition strength of $\sim$0.1 W.u. would be expected [31]. Similarly, the implied strength for a 573.5-keV $M2$ is lower than allowed $M2$ values but it is also higher than a typical j-forbidden $M2$ transition strength. In any case, a 22^+ assignment for the isomer at 4417 keV seems unlikely. Indeed, one of the main problems of a 22^+ assignment is that a range of favored $E2$ and $M1$ transitions would be expected, for instance, a 712-keV $E2$ γ-ray between the state at 3754 keV and the state at 3041 keV. Such transitions are not seen in our study. Similarly, one would expect the branching ratio of the observed 517.2-keV γ ray to be much bigger than is measured.

Consequently, the favored scenario is that both lines at 573.5 and 663.3 keV are $E3$ transitions, with the slower transition rate of the 663.3 keV still not fully understood, even though we suggest that it could be explained by configuration mixing. Conclusive assignments could be provided by more precise measurement of the internal conversion coefficients.

2. The isomer at $E_x = 2206$ keV

The 15^- isomer at 2206 keV, $\tau = 1.79(11)$ ns, can be related to similar isomers in ^{211}Fr, ^{212}Fr, and ^{213}Fr at 2538 ($J^\pi = 29/2^+$), 2492 ($J^\pi = 15^-$), and 2423 keV ($J^\pi = 29/2^+$), respectively (see Ref. [8]). In those three isotopes, the isomers decay by either an $E3$ (^{212}Fr and ^{213}Fr) or by an $E3$ and an $E2$ transition (^{211}Fr). As the neutron number decreases, the energy of the 14^- state lowers and in ^{210}Fr the state is low enough that the $E1$ decay is favored over higher multipolarities. This explains the factor of 10^2–10^3 between the lifetime measured in ^{210}Fr compared to the three higher mass isotopes. The configuration assignment for the isomer is $\pi(h_{9/2}^4 i_{13/2})_{9/2} \otimes \nu p_{1/2}^{-2} f_{5/2}^{-1}$.

3. The isomer at $E_x = 2018$ keV

The 11^- isomer observed at 2018 keV has no equivalent state in neighboring nuclei. The semiempirical shell-model calculation predicts an 11^- state from the $\pi h_{9/2}^5 \otimes \nu(p_{1/2}^{-2} i_{13/2}^{-1})$ configuration that is in good agreement with the observed energy (see Fig. 16). The isomer decays via a 1176-keV $M2$ transition, for which the strength has been measured at $\sim$0.04(1) W.u. (see Table III). The neutron configuration of the final 9^+ state at 842 keV is $\nu(p_{1/2}^{-2} f_{5/2}^{-1})$ while that of the isomer is almost certainly $\nu(p_{1/2}^{-2} i_{13/2}^{-1})$. The protons are likely to be passive spectators for this transition, but, regardless of their actual behavior an $M2$ transition between these states is j forbidden. Thus, a transition strength of $\sim$10^{-3} W.u. is expected [15]. The measured value of 4×10^{-2} W.u. is slightly higher, but remains plausible. The

TABLE V. Transition strengths for decays from 10^- isomers in odd-odd bismuth, astatine, and francium nuclei.

Nucleus[a] state	Initial state, τ	Final state, J^π	E_γ (keV)	I_γ	$\sigma\lambda$	α_T [b]	Transition strength (W.u.)
^{204}Bi	808 keV, 13 ms						
		7^+	752	100	$E3$	0.0326	3.87×10^{-4}
^{206}Bi	1043 keV, 0.88 ms						
		7^+	904	60	$E3$	0.0207	1.97×10^{-4}
		8^+	229	80	$M2$	4.26	3.85×10^{-4}
^{206}At	808 keV, 1173 ns						
		7^+	122	100	$E1$	0.282	1.03×10^{-7}
^{208}At	1090 keV, 45 ns						
		7^+	1019	0.7	$E3$	0.0175	8.40×10^{-2}
		9^+	187	100	$E1$	0.0990	8.53×10^{-7}
^{208}Fr	826 keV, 623 ns						
		9^+	194	100	$E1$	0.0947	5.56×10^{-8}
^{210}Fr	1113 keV, 29.8 ns						
		9^+	271	100	$E1$	0.0431	4.49×10^{-7}

[a]References: ^{204}Bi [34], ^{206}Bi [34], ^{206}At [16], ^{208}At [27], ^{208}Fr [16], ^{210}Fr [present work].
[b]Values taken from Ref. [25].

level scheme could be inaccurate in this region; however, the J^π assignment is possible as a lower spin would mean the state is far off the yrast line and should not be strongly populated.

4. The 10^- isomer at $E_x = 1113$ keV

The 10^- isomer at 1113 keV in ^{210}Fr decays via an $E1$ transition and is almost certainly from the $\pi(h_{9/2}^5)_{9/2} \otimes \nu(j^{-2})_0 i_{13/2}^{-1}$ configuration. The observed hindrance of 2×10^6 is consistent with typical $E1$ transition strengths observed in the lead region, and it is also similar to what has been observed in other odd-odd nuclei in this region (see Ref. [32] and Table V). The 9^+ state, at 842 keV, would be from the $\pi(h_{9/2}^4) \otimes \nu(p_{1/2}^{-2} f_{5/2}^{-1})$ or $\pi(h_{9/2}^4 f_{7/2}) \otimes \nu(p_{1/2}^{-2} f_{5/2}^{-1})$ configurations (or an admixture). Consequently, the difference in the neutron-hole orbital angular momentum between the initial and final states is bigger than the angular momentum carried by the $E1$ γ ray (hence j-forbidden) and this explains the typical observed hindrance of 10^6–10^7 [32]. The energy of the isomer is related to the $i_{13/2}^{-1}$ neutron-hole energy in odd Pb isotopes (note that a $13/2^+$ isomer is observed in neutron-deficient odd-even nuclei in the Pb region) that falls with neutron number quite rapidly, while the 9^+ state energy depends on details of the proton-excitation because the neutrons are still in the ground-state configuration. This is shown in Fig. 17, where it can be seen that the energy of the isomer depends on the neutron number while it is almost constant as the proton number increases.

As one moves to more neutron-deficient isotopes, the energy of the 10^- isomer can potentially fall lower, below the 9^+ state, such that it can only decay via an $E3$ transition. Such an $E3$ transition was first observed in ^{208}Bi [33]; however, if the 10^- state stays close to, but above, the 9^+ state, then one may expect both $E1$ and $E3$ decays to proceed. This is observed in ^{204}Bi and ^{206}Bi, but a very weak $E3$ γ ray has also been observed in ^{208}At by Fant *et al.* [27]. In ^{210}Fr, the energy gap between the 10^- state at 1113 keV and the 9^+ state at 842 keV

means that the $E1$ transition will dominate over the $E3$ transition, in agreement with our measurements. Evaluating the $E1$-to-$E3$ transition rate in ^{208}At, the corresponding $E3$ γ ray in ^{210}Fr would have a strength of $\sim4.5\times10^{-2}$ W.u. and therefore the branching ratio with the $E1$ transition would be $\sim$1:250.
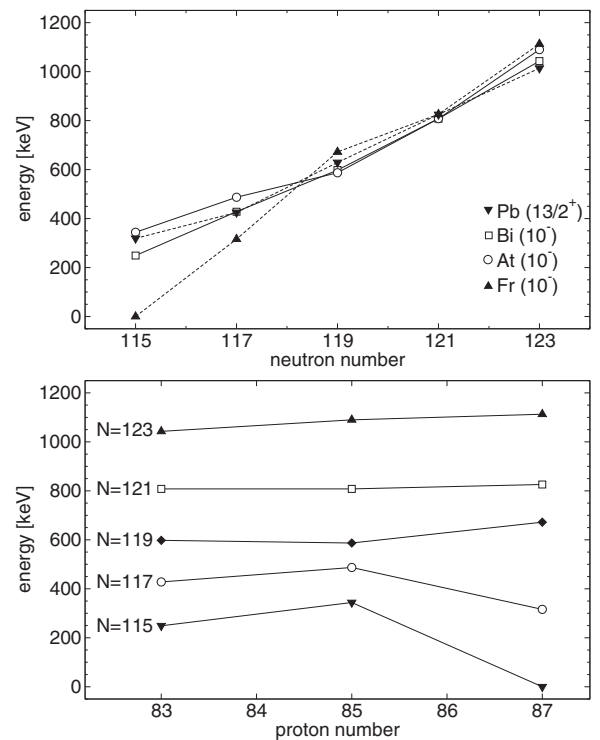

FIG. 17. A comparison for selected nuclei of the energy of the 10^- isomer for odd-odd isotopes and the $13/2^+$ isomer for even-odd isotopes is shown in the top panel. A similar comparison for isotonic chains is shown in the bottom panel. The points for $Z = 82$ represent the $13/2^+$ isomer energy in lead isotopes.

V. CONCLUSION

The structure of ^{210}Fr has been investigated and for the first time a rigorous level scheme of yrast and near yrast levels up to an energy of 5.5 MeV and spin/parity of (26$^-$) is reported. The extensive empirical shell-model calculations performed provide a weaker agreement with the experimental values than that found, for similar calculations, nearer to the closed shells. It is plausible that the lower agreement is attributable to mixing of configurations, a feature that cannot be included for ^{210}Fr owing to the extreme size of the calculation space. However, some well-known and expected features, such as the 10$^-$ isomer at 1113 keV, are very well understood. A high-spin, long-lived isomer at 4417 keV is understood to arise from the $\pi(h_{9/2}^3 i_{13/2}^2) \otimes \nu(p_{1/2}^{-2} f_{5/2}^{-1})$ configuration, although the exact angular momentum and the multipolarity of the decay transitions are still open questions. If the two $E3$ assignments for the transitions at 573.5 and 663.3 keV are confirmed, this would be a rare case of a high-spin isomer in the trans-lead region decaying via two $E3$ transitions. Although the $B(E3)$ values are somewhat different from the usual values, tangible explanations, using configuration mixing, have been presented. These fit well with the systematics of the region and give a natural explanation of the level scheme. We therefore favor the (23)$^+$ assignment.

[1] I. Hamamoto, Phys. Rep. **10**, 63 (1974).
[2] T. T. S. Kuo and G. H. Herling, NRL Report No. 2258, Naval Research Laboratory, Washington, 1971.
[3] S. Bayer, A. P. Byrne, G. D. Dracoulis, A. M. Baxter, T. Kibédi, F. G. Kondev, S. M. Mullins, and T. R. McGoram, Nucl. Phys. A **650**, 3 (1999).
[4] B. Szpak, K. H. Maier, A. S. Smolkowska, B. Fornal, R. Broda, M. P. Carpenter, N. Cieplicka, R. V. F. Janssens, W. Krolas, T. Pawlat, J. Wrzesinski, and S. Zhu, Phys. Rev. C **83**, 064315 (2011).
[5] K. H. Maier, T. Kibédi, G. D. Dracoulis, P. Boutachkov, A. Aprahamian, A. P. Byrne, P. M. Davidson, G. J. Lane, M. Marie-Jeanne, P. Nieminen, and H. Watanabe, Phys. Rev. C **76**, 064304 (2007).
[6] K. H. Maier and M. Rejmund, Eur. Phys. J. A **14**, 349 (2002).
[7] S. Bayer, A. P. Byrne, G. D. Dracoulis, A. M. Baxter, T. Kibédi, and F. G. Kondev, Nucl. Phys. A **694**, 3 (2001).
[8] A. P. Byrne, G. D. Dracoulis, C. Fahlander, H. Hübel, A. R. Poletti, A. E. Stuchbery, J. Gerl, R. F. Davie, and S. J. Poletti, Nucl. Phys. A **448**, 137 (1986).
[9] A. P. Byrne *et al.*, Phys. Lett. B **217**, 38 (1989).
[10] A. P. Byrne, G. J. Lane, G. D. Dracoulis, B. Fabricius, T. Kibédi, A. E. Stuchbery, A. M. Baxter, and K. J. Schiffer, Nucl. Phys. A **567**, 445 (1994).
[11] M. W. Drigert, J. A. Cizewski, and M. S. Rosenthal, Phys. Rev. C **32**, 136 (1985).
[12] L. P. Gaffney, P. A. Butler *et al.*, Nature (London) **497**, 199 (2013).
[13] M. E. Debray, J. Davidson, M. Davidson, A. J. Kreiner, D. Hojman, D. Santos, K. Ahn, D. B. Fossan, Y. Liang, R. Ma, E. S. Paul, W. F. Piel, and N. Xu, Phys. Rev. C **41**, R1895 (1990).
[14] D. A. Meyer, C. W. Beausang, J. J. Ressler, H. Ai, H. Amro, M. Babilon, R. F. Casten, C. R. Fitzpatrick, G. Gürdal, A. Heinz, E. A. McCutchan, C. Plettner, J. Qian, N. J. Thomas, V. Werner, E. Williams, N. V. Zamfir, and Jing-ye Zhang, Phys. Rev. C **73**, 024307 (2006).
[15] G. D. Dracoulis, P. M. Davidson, G. J. Lane, A. P. Byrne, T. Kibédi, P. Nieminen, H. Watanabe, and A. N. Wilson, Phys. Rev. C **79**, 054313 (2009).
[16] G. D. Dracoulis, P. M. Davidson, G. J. Lane, A. P. Byrne, T. Kibédi, P. Nieminen, A. N. Wilson, and H. Watanabe, Eur. Phys. J. A **40**, 127 (2009).
[17] D. J. Hartley, E. P. Seyfried, W. Reviol, D. G. Sarantites, C. J. Chiara, O. L. Pechenaya, K. Hauschild, A. Lopez-Martens, M. P. Carpenter, R. V. F. Janssens, D. Seweryniak, and S. Zhu, Phys. Rev. C **78**, 054319 (2008).
[18] D. Kanjilal, S. Saha, S. Bhattacharya, A. Goswami, R. Kshetri, R. Raut, S. Muralithar, R. P. Singh, G. Mukherjee, and B. Mukherjee, Phys. Rev. C **84**, 064321 (2011).
[19] V. Margerin, G. J. Lane, G. D. Dracoulis, N. Palalani, and M. L. Smith, EPJ Web Conf. **35**, 06003 (2012).
[20] G. D. Dracoulis and A. P. Byrne, Annual Report ANU-P/1052, 115, 1989.
[21] A. R. Poletti, G. D. Dracoulis, S. J. Poletti, A. P. Byrne, A. E. Stuchbery, and J. Gerl, Nucl. Phys. A **442**, 153 (1985).
[22] S. Bayer, A. P. Byrne, and G. D. Dracoulis, Nucl. Phys. A **591**, 104 (1995).
[23] P. Kuusiniemi, F. P. Heßberger, D. Ackermann, S. Hofmann, and I. Kojouharov, Eur. Phys. J. A **22**, 429 (2004).
[24] V. Margerin, Master of Philosophy thesis, Australian National University, 2012; https://digitalcollections.anu.edu.au/handle/1885/101020.
[25] T. Kibédi, T. W. Burrows, M. B. Trzhaskovskaya, P. M. Davidson, and C. J. Nestor, Jr., Nucl. Instrum. Methods A **589**, 202 (2008).
[26] C. Ekström, S. Ingelman, G. Wannberg, and M. Skarestad, Phys. Scr. **18**, 51 (1978).
[27] B. Fant, T. Weckström, T. Lönnroth, C. J. Herrlander, K. Honkanen, and A. Källberg, Nucl. Phys. A **429**, 296 (1984).
[28] J. Blomqvist, P. Kleinheinz, and P. J. Daly, Z. Phys. A **312**, 27 (1983).
[29] A. R. Poletti, G. D. Dracoulis, C. Fahlender, and A. P. Byrne, Nucl. Phys. A **440**, 118 (1985).
[30] I. Bergström and B. Fant, Phys. Scr. **31**, 26 (1985).
[31] A. P. Byrne, Ph.D. thesis, Australian National University, 1986.
[32] T. Lönnroth, Z. Phys. A **331**, 11 (1988).
[33] M. Bonitz, J. Kantele and N. J. Sigurd Hansen, Nucl. Phys. A **115**, 219 (1968).
[34] Y. N. Rakivnenko, A. P. Klyucharev, V. A. Lutsik, I. A. Romanii, E. A. Skakun, and G. I. Yatsenko, Yad. Fiz. **20**, 617 (1974).